PROCEEDINGS, 48th Workshop on Geothermal Reservoir Engineering
Stanford University, Stanford, California, February 6-8, 2023
SGP-TR-224

Monte Carlo Model Simulations of Tracer Tests to Determine Fracture Aperture Size Range in an Anisotropic Geothermal Reservoir

Selçuk Erol[1], Taylan Akın[2] and Serhat Akın[3]

[1]Energy Systems Engineering Department, İzmir Institute of Technology, İzmir, Turkey

[2]Geothermal Application & Research Center, Pamukkale University, Denizli, Turkey

[3]Petroleum and Natural Gas Engineering Department, Middle East Technical University, Ankara, Turkey

selcukerol@iyte.edu.tr

Keywords: Tracer test, analytical model, fractured reservoirs, dispersion, GECO

ABSTRACT

The predictive modeling of flow and transport processes in geothermal reservoirs is challenging due to the complex nature of fracture networks. Tracer tests are traditionally used to characterize such reservoirs for sustainable injection and production strategies. Interpretation of tracer tests for acquiring correct flow parameters is usually carried out using oversimplified mathematical models. The analytical approaches particularly developed for modeling tracer tests in porous and fractured media provide uniform flow parameters that are not suitable for detailed geothermal reservoir characterization due to anisotropy and macro-dispersion. Moreover, numerical dispersion parameters that represent the macro-dispersion of a tracer are usually not pertinent. In this study, a tracer test is analyzed to characterize and predict the thermal breakthrough time of a geothermal reservoir located in western Turkey. A new analytical model particularly developed for the analysis of tracer tests conducted in porous and fractured reservoirs is coupled with Monte-Carlo simulations acquiring effective parameters from well-to-well data to obtain fracture aperture values in an anisotropic fractured medium. Subsequently, fracture aperture values are evaluated by analyzing mud-loss data provided by well-logs and compared with the analytical model results. The objective is to estimate the fracture aperture size and to inspect the relationship between anisotropic flow, fracture aperture orientation, and longitudinal dispersivity in a deep geothermal reservoir. Results demonstrate that the anisotropic flow paths have an impact on the macro-dispersivity both in longitudinal and transversal directions.

1. INTRODUCTION

The use of tracer tests to estimate the progression of the cold front between injection and production wells, as well as energy depletion, is critical. Therefore, quantitative characterization of flow, transport mechanisms, and interpretation of tracer test results are important issues in a deep geothermal reservoir.

Computer-based models may be used to examine the tracer transport process, and important reservoir parameter values can be obtained through calibration using field responses. Analytical models based on solutions of the convection-dispersion-diffusion differential equation are commonly used (Sauty 1980; Bullivant & O'Sullivan, 1989; Maloszewski & Zuber, 1993; Gerke & van Genuchten, 1996; Cihan & Tyner, 2011; Houseworth et al., 2013; Somogyvári & Bayer, 2017). One of the major problems is that geothermal reservoirs have mostly a strong anisotropy for the flow due to differing rock types and the presence of oblique fault angles, and the injected tracer is strongly dispersed. One-dimensional (1-D) or two-dimensional (2-D) radial symmetry is a typical assumption for such analytical models. For anisotropic porous and fractured media, lower-dimensional models give very limited isotropic information. Full 3-D numerical models can be used as an alternative to radial analytical simulation, but they demand a significant amount of processing time and data (Cihan & Tyner 2011; Egert et al, 2020; Wu et al., 2021). Erol et al. (2022) recently developed a 3-D analytical model that accounts for anisotropy and dispersivity to reduce the computational effort of implementation and calibration. This model allows for inspecting anisotropic reservoir characteristics and examining the distribution of solute residence time. In this study, the developed novel analytical model combined with Monte-Carlo simulations to estimate fracture aperture values in an anisotropic fractured medium will be presented. The analytical model is iteratively fitted to tracer breakthrough curve (BTC) data collected at production wells of the Kızıldere geothermal field located in the Büyük Menderes Graben in western Turkey (Şimşek et al., 2005). In addition, fracture aperture values are evaluated by analyzing mud-loss data obtained from the well log and compared with the analytical model results. The overall aim of this research is to assess the relationship between anisotropic flow, hydraulic aperture orientation, and longitudinal dispersivity in a deep geothermal reservoir.

2. METHODOLOGY

2.1 Analytical model and Monte-Carlo simulations

The 3-D analytical model developed for anisotropic media to extract effective parameters from well-to-well data is used in this study. This model is derived based on Green's function approach to generate an analytical 3-D convection-dispersion equation. The moving line source idea is applied to solve Green's function for anisotropic media. Afterward, a rectangular injection function and Green's function of 3-D solute transport are analytically convoluted to represent a pulse injection.

A continuous medium approach serves as a basis for the description of transport in fractured reservoirs. The governing partial differential equation (PDE) of the solute convection-dispersion-diffusion in 3-D cartesian coordinates in continuum media is given as (Leij et al. 2000):

$$R\frac{\partial c}{\partial t}=\left(D_x\frac{\partial^2 c}{\partial x^2}+D_y\frac{\partial^2 c}{\partial y^2}+D_z\frac{\partial^2 c}{\partial z^2}\right)-u_x\frac{\partial c}{\partial x}-u_y\frac{\partial c}{\partial y}-u_z\frac{\partial c}{\partial z}+s \tag{1}$$

where t is time, c is the solute concentration, R is the solute retardation factor, $D_{x,y,z}$ are hydrodynamic dispersion coefficients, u_x, u_y and u_z are flow velocities along the x-, y-, and z-directions, and s is the production term.

Hydrodynamic dispersion coefficients are calculated based on longitudinal α_L and transverse α_T macro-dispersivities that are defined in the x-, y-, and z-directions as follows:

$$D_x=D_0+\alpha_L u_x;\; D_y=D_0+\alpha_T u_y;\; D_z=D_0+\alpha_T u_z \tag{2}$$

in which D_0 is the molecular diffusion coefficient. The dispersivities depend on the velocity field. The x-direction is considered longitudinal, and the y- and z-directions are transversal.

The Green's function of a pulse point source is obtained by Leij et al., (2000) at the given point coordinates (x', y', z') and time $t = 0$ by solving the fundamental formulation of the PDE given in equation (1). In the following step, the moving source theory for the x-, y-, and z-directions with constant drifts is applied (Carslaw & Jaeger, 1959). After applying the superposition technique for a finite length of a wellbore representative for the perforated well depth. After the integration by using the substitution method and simplification, the governing equation is reduced to:

$$F=\frac{C_L R}{8\pi t\sqrt{D_x D_y}}\exp\left(\frac{\left(R\left(x-x'\right)-v_{Tx}t\right)^2}{4tD_x R}-\frac{\left(R\left(y-y'\right)-v_{Ty}t\right)^2}{4tD_y R}\right)\times\left(erf\left(\frac{R\left(H-z\right)+tv_{Tz}}{\sqrt{4tD_z R}}\right)-erf\left(\frac{tv_{Tz}-Rz}{\sqrt{4tD_z R}}\right)\right) \tag{3}$$

where v_{Tx}, $v_{Ty,}$ and v_{Tz} are the solute velocities, which yield the flow velocity vector:

$$v_{Tx,y,z}=\frac{\mathrm{Pe}_{x,y,z}D_0}{h}=\underbrace{\frac{u_{x,y,z}L}{D_0}}_{\mathrm{Pe}_{x,y,z}}\frac{D_0}{h} \tag{4}$$

where L is the characteristic length, and h is the fracture aperture.

C_L given in equation (3) is a Heaviside step function where $C_L(t) = 1$, for $t \geq 0$. If C_L is superimposed per meter depth for a given time. The input rectangular pulse injection function is analytically convoluted by shifting over the convection-dispersion-diffusion part of equation (3) (impulse response) with a given time interval Δt.

This convolution method is carried out by segregating equation (3) into two parts: c_L represents a rectangular pulse function, and the convection-dispersion-diffusion part is expressed as an impulse response function I (x, y, z, t). Hence, the following equation can be obtained:

$$c\left(x,y,z,t\right)=c_L\underbrace{\left\{\begin{array}{l}\dfrac{R}{8\pi t\sqrt{D_x D_y}}\exp\left(\dfrac{\left(R\left(x-x'\right)-v_{Tx}t\right)^2}{4tD_x R}-\dfrac{\left(R\left(y-y'\right)-v_{Ty}t\right)^2}{4tD_y R}\right)\\ \times\left(erf\left(\dfrac{R\left(H-z\right)+tv_{Tz}}{\sqrt{4tD_z R}}\right)-erf\left(\dfrac{tv_{Tz}-Rz}{\sqrt{4tD_z R}}\right)\right)\end{array}\right\}}_{I(x,y,z,t)} \tag{5}$$

The convolution of the function I and c_L can be formulated by applying a pulse injection for a specific time frame in which T is the period of rectangular pulse injection, c_L is the injected tracer concentration rate per meter depth that can be given as:

$$c(x,y,z,t)=\int_{-\infty}^{\infty} c_L(\tau)\,I(x,y,z,t-\tau)d\tau \rightarrow c_L\int_0^{T} I(x,y,z,t-\tau)d\tau \tag{6}$$

This convolution integral equation can be solved by discretizing both the c_L and I function with a differential interval of Δt. The sum of impulse responses at given coordinates (x, y, z) provides the convolution in analytical form and can be written as:

$$c(x,y,z,t)=\sum_{i=0}^{n-1} c_L(i\Delta t)\,I(x,y,z,t-i\Delta t)\Delta t \tag{7}$$

This convolution integral equation can be solved by discretizing both the c_L and I function with a differential interval of Δt. The sum of impulse responses at given coordinates (x, y, z) provides the convolution in analytical form and can be written as:

$$c(x,y,z,t)=\sum_{i=0}^{n-1} c_L(i\Delta t)\,I(x,y,z,t-i\Delta t)\Delta t \tag{8}$$

where $i\ \Delta t$ denote the time interval of each unit impulse (i.e., time delay), n is the period, and the delayed and shifted impulse response is expressed as $c_L(i\ \Delta t)\ I(t - i\ \Delta t)\ \Delta t$. This analytical model given in equation [8] is called Anisotropic Solute Moving Line Source (ASMLS).

This analytical model is implemented in an exhaustive Monte-Carlo analysis to identify feasible ranges and distributions of anisotropic flow velocities, fracture aperture, and longitudinal and transversal dispersivities. In this analysis, a sufficiently large number of uncertain model parameter values is randomly generated by sampling from predefined distributions. Each sample simulation is tested by computing a square error function to quantify the fitness between the calculated and measured tracer BTCs. Feasible parameter ranges are identified by selecting a set of best-fit results.

We defined a triangular probability distribution function in the Monte-Carlo simulations as:

$$P_j(i)=P_{j\_\min}+X\left(P_{j\_\max}-P_{j\_\min}\right) \tag{9}$$

P is the value of the desired parameter for estimation, bounded with upper and lower limits; X is a continuous random variable of a probability density function that generates random numbers for each iteration within the range $0 < X < 1$. The subscript j denotes the parameter, i is the number of realizations. The square error function is defined as (Wu et al., 2021):

$$R_j(i)=\frac{1}{\xi_e^2}\left[\left(\frac{c_{i\_peak}}{c_{mea\_peak}}-1\right)^2+\left(\frac{t_{i\_peak}}{t_{mea\_peak}}-1\right)^2+\left(\frac{t_{i\_1}}{t_{mea\_1}}-1\right)^2+\left(\frac{t_{i\_2}}{t_{mea\_2}}-1\right)^2\right] \tag{10}$$

the subscript i denotes the Monte-Carlo simulation results, *mea* the measured data, *peak* the maximum value of the concentration. The corresponding arrival time is t_{peak}; t_1 and t_2 are the beginning and the end of the BTC, respectively. For each realization, we found the beginning and the peak of the BTC. The beginning and the end of the curve are determined in an iterative process. In the first step, a threshold value is set (e.g., 0.1) and concentrations larger than the threshold value are determined. In the second step, the large value differences along the dataset array are evaluated, and the indices of the high difference points on the curve are found at the beginning and the end of the curves.

ξ_e is the standard error of the mean that can be estimated as:

$$\xi_e=\frac{\xi}{\sqrt{N}} \tag{11}$$

ξ is the standard deviation of the measurement dataset in dimensionless form (c/c_{max}) and N is the number of measured data.

2.2. Fracture aperture evaluation with mud-loss data

To compare the results obtained from the ASMLS model, fracture apertures are estimated using mud-loss data from the wells. Mud invasion from a wellbore into the surrounding formation can be used to determine fracture apertures of the formations. Huang et al. (2011) developed a method for estimating fracture aperture size that involves solving a quadratic equation with wellbore radius, overpressure ratio, and the maximum mud-loss volume as input parameters. According to this approach, it is assumed that mudflow will stop in time due to overpressure reaching to yield stress of the drilling fluid. The ultimate invasion radius of mudflow (equation [12]) depends on the wellbore radius r_w (m), fracture aperture h (m), the yield stress of the mudflow τ_y (Pa), and pressure difference from the well to the formation ΔP (Pa).

$$(r_s)_{\max}=1+\frac{h\Delta P}{3r_w\tau_y} \tag{12}$$

Maximum mud-flow volume (m^3) is given as

$$\left(V_m\right)_{\max} = \pi h\left(\left(r_s\right)^2_{\max} - r_w^2\right) \tag{13}$$

A combination of equation (12) and equation (13) gives the quadratic equation (Huang et al., 2011)

$$\left(\frac{\Delta P}{\tau_y}\right)^2 h^3 + 6r_w\left(\frac{\Delta P}{\tau_y}\right)h^2 - \frac{9}{\pi}\left(V_m\right)_{\max} = 0 \tag{14}$$

where $\Delta P/\tau_y$ is the overpressure ratio. Maximum mud-loss volume can be determined using total mud-loss volume over the number of events of mud-losses in a given time.

3. CASE STUDY

The study is carried out at the Kızıldere geothermal field located in the Denizli and Aydın provinces of western Turkey (Aydın et al. 2020). The geothermal reservoir consists of metamorphic rocks with faults and fracture networks.

The field is considerably large and lies over an area of more than 250 km^2, therefore, we only focus on a part of the geothermal field where the injection and production activities are intensive. The Kızıldere field is bounded by oblique-slip normal faults with various orientations. Based on the geological model of the Kızıldere geothermal field, four major faults generate a combination of sinks and sources between shallow and deep hydrothermal reservoirs in the local area of interest (Figure 1a).

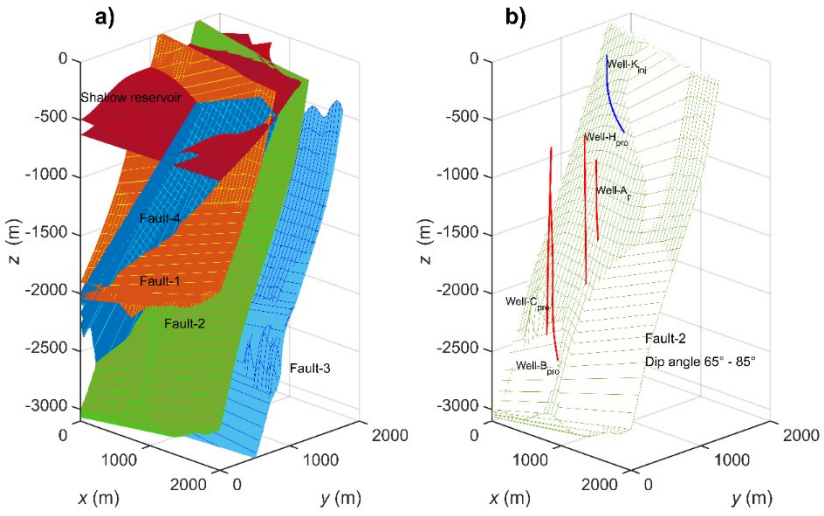

Figure 1: a) Geological settings and the major fault zones of the survey zone in the Kızıldere geothermal reservoir. The highlighted red color surface defines the lower boundary of the shallow reservoir. b) Illustration of the injection (blue) and production (red) wells intersecting fault-2.

These combined fluxes result in various anisotropic flow paths in different directions and complicate the estimation of representative reservoir parameters. Our particular interest is in a single fault zone (fault-2) that is intersected by four production and one injection wellbore, as shown in Figure1b. The injection was carried out at the shallower well and monitored from the deeper production wells along the fault-2. This tracer survey is suitable to examine the ASMLS model. For our study, the four production wells located closely to the injection wells were considered.

The reservoir temperature is about 250 °C at around 2000 m depth (Şimşek, 2003). A mass of 200 kg of 1-naphthalene sulfonate, whose thermal decay kinetics are suitable for use in reservoirs with temperatures up to 300 °C (Rose et al., 2001), was mixed with the effluent fluid and injected into the injection well Well-K_{inj}.

The tracer was injected in less than an hour. In the ASMLS model, the line source length H is specified based on the perforated depth of the injection well and it is assumed that the tracer is uniformly injected along the fully penetrated perforation depth. The total amount of tracer injected in one hour into Well-K_{inj} is simply divided by the perforated depth of Well-K_{inj} as 150 m, which means that c_L must be specified as 1.33×10^6 mg m^{-1} h^{-1} in the ASMLS model depending on the time interval in the convolution (i.e., 370 mg m^{-1} s^{-1}).

4. RESULTS

The ASMLS model is coupled with Monte-Carlo simulations to evaluate values for the unknown parameters in the form of distributions. In the ASMLS model, there are eight unknown parameters (flow velocities and fracture aperture in x, y, z directions, and dispersivities) to assess with Monte-Carlo simulations. In each trial, the calculated results are fitted to the measured tracer data monitored in other observation wells shown in Figure 1b. The calibration is applied for each observation well couple separately (e.g., Well-K_{inj} to -A_{pro}, Well-K_{inj} to -$B_{pro,}$ etc.). The concentrations are calculated at the Cartesian point coordinates nearest to the observation well where fault-2 is intersected.

Firstly, global sensitivity analysis is carried out with 50,000 realizations to determine the average ranges of each parameter between the injection and observation wells (for Well-A_{pro}, Figure 2). Then, in 5,000 realizations, the sensitivity of each parameter was tested following a one-at-a-time principle: the value limits of the concerned parameter were set in a wide range, while those of the other parameters were kept narrow (Figure 3). For instance, the flow velocity in the *x*-direction is analyzed within the limits from 1×10^{-7} to 1×10^{-3} m s^{-1}, while for other parameters such as longitudinal dispersivity a tight limit of 200 to 300 m is set, and the other velocities are bounded between 1×10^{-6} and 1×10^{-5} m s^{-1}. Once the limits are restricted for the flow velocity components, the size of the fracture apertures in three directions is estimated.

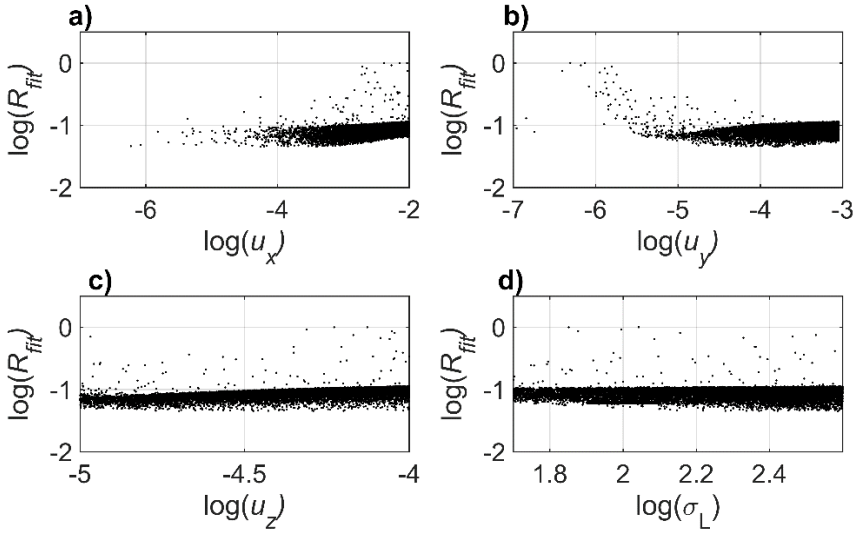

Figure 2: Monte-Carlo simulation results of the tracer transport (Well-Apro). Tracer was injected into Well-Kinj. The misfit function Rfit is plotted as a function of flow velocity in x-, y- and z-directions (a, b and c), longitudinal dispersivities (d). Each point represents a realization.

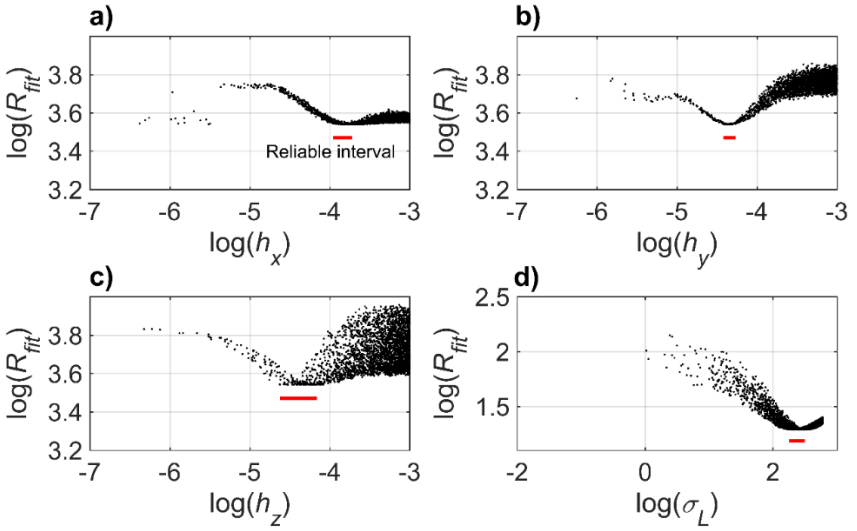

Figure 3: Monte-Carlo simulation results of the tracer transport (Well-B_{pro}). The misfit function R_{fit} is plotted as a function of fracture aperture in x-, y- and z-directions (a, b, and c), and longitudinal dispersivity (d). Each point represents a realization. Tracer was injected into Well-K_{inj}.

In Figure 3, fracture apertures between the Well-K_{inj} and -B_{pro} in three directions are estimated with a one-at-a-time principle and the feasibility ranges of parameters are evaluated at a more optimal point. The fracture apertures h_x, h_y, and longitudinal dispersivity α_L are at a clearer feasibility range on the misfit function R_{fit} whereas h_z shows a wider range of feasibility due to the vertical heterogeneity. In other wells, we observed extensive feasibility ranges for fracture aperture in different directions as the distance between the injection and the observation wells becomes more significant (Table 1). As the distance gets longer, the concentration levels measured in the field are relatively low due to dispersion which complicates the assessment of fitting parameters.

Results for fracture apertures are reported in Table 1. The estimated fracture apertures with mud-loss data are consistent with the fracture aperture in the *x*-direction obtained with the ASMLS model. Flow velocities are mainly stimulated by the forced convection between the injection and production (tracer observation) wells. The flow velocity in the *x*-direction is one order of magnitude faster compared to *y*- and *z*-directions, but the observation wells are located in *y*- and *z*-axes directions where the velocity is slower. In contrast, we found that absolute permeability calculated based on Darcy's law is larger in the *y*- and *z*-axes. The reason is that the pressure gradient is small (i.e., low-pressure gradient). In addition, the fault-2 orientation is perpendicular to the surface with a dip angle between 65 º - 85 º, and the fracture aperture in the *y*- and *z*-directions are significantly larger which dissipates the flow in 3D. This leads to a larger macro-dispersion both in longitudinal and transversal directions in the reservoir. In an isotropic homogeneous medium, the vertical transverse dispersivity is typically an order of magnitude smaller than longitudinal dispersivity. During the Monte-Carlo application of the ASMLS model, the feasible range is obtained with a transversal dispersivity that is around 0.4 times smaller than the longitudinal dispersivity. Therefore, larger macro-dispersivity may indicate a strong anisotropic behavior.

Table 1. Monte-Carlo simulation results between fracture apertures obtained in an anisotropic medium with the ASMLS model and fracture apertures estimated based on the mud-loss data.

From Well-K_{inj} to other wells	Distance at *z*-direction - (m)	ΔP [a] (bar)	Depth range of perforated depth	Fracture aperture (μm) mud-loss [b]	Fracture aperture (μm) ASMLS model [c]			Dispersivities (m)	
				h_m	h_x	h_y	h_z	α_L	α_T
Well-A_{pro}	750	70	1750 - 1900	120 - 170	70 - 140	55 - 85	65 - 95	220 - 250	α_L×0.4
Well-H_{pro}	1000	80	2000 - 2200	40 - 220	75 - 125	20 - 30	30 - 50	220 - 260	α_L×0.4
Well-C_{pro}	1500	100	2200 - 2400	70 - 220	140 - 380	40 - 75	20 - 400	240 - 260	α_L×0.4
Well-B_{pro}	1600	110	2100 - 2700	90 - 130	110 - 190	40 - 55	25 - 70	240 -260	α_L×0.4

[a] Pressures are obtained after the hydraulic regime has reached steady-state conditions. [b] Fracture aperture h_m estimated with mud-loss data of the wells. [c] Fracture apertures in three directions were obtained by matching tracer measurements with minimum square root error between Well-K_{inj} and the production wellbores with the ASMLS model.

4. CONCLUSION

A novel analytical model developed for tracer injection to inspect solute transport in an anisotropic medium is utilized to evaluate longitudinal macro-dispersivity and fracture apertures in three directions. Monte-Carlo simulation algorithm is then implemented to determine optimal values for unknown reservoir parameters, particularly, the fracture apertures in *x*-,*y*-, and *z*-directions. Moreover, fracture aperture values estimated by assessing mud-loss data obtained from the well-log are compared with the analytical model results.

The geothermal reservoir consists of metamorphic rocks that typically exhibit strong anisotropic behavior affecting the flow propagation. In the reservoir, the tracer injection and monitoring were carried out to inspect the course of energy depletion and to determine related anisotropic reservoir parameters. It is assumed that the flow is most dominant on a major fault with a dip angle of 65º to 85º that intersects the injection and the observation wells. The estimated fracture aperture with mud-loss data is mostly consistent with the fracture aperture in the *x*-direction obtained with the ASMLS model in Cartesian coordinates. In addition, the fracture apertures in the *y*- and *z*-directions are also moderately effective and drive and disperse the flow in three directions. This demonstrates that the injected tracer propagates dominantly in the *x*-direction but the flow paths on the *y*- and *z*-direction significantly affect the dispersion of the tracer both in longitudinal and transversal directions in an anisotropic medium.

ACKNOWLEDGMENT

This paper presents the results of the GECO Project, funded by the European Union's Horizon 2020 research and innovation program under grant agreement No. 818169. The authors would like to thank ZORLU Energy for the tracer data and the well-log data.

REFERENCES

Aydın, H., Akın, S., and Şentürk, E.: Evaluation of Production Capacity of Geothermal Power Plants in Turkey. *GRC Transactions*, 44, (2020)

Bullivant, D. P., and O'Sullivan, M., J.: Matching a field tracer test with some simple models, *Water Resources Research*, 25(8), (1989), 1879– 1891.

Carslaw, H. S., and Jaeger, J.C.: Conduction of Heat in Solids, 2nd Edition. *Oxford University Press*, New York, US, (1959).

Cihan, A., and Tyner, J. S.: 2-D radial analytical solutions for solute transport in a dual-porosity medium, *Water Resources Research*, 47, (2011), W04507.

Egert, R., Korzani, M. G., Held, S., Kohl, T.: Implications on large-scale flow of the fractured EGS reservoir Soultz inferred from hydraulic data and tracer experiments. *Geothermics*, 84, (2020), 101749.

Erol, S., Bayer, P., Akın, T., and Akın, S.: Advanced workflow for multi-well tracer test analysis of a geothermal reservoir. *Geothermics*, 101, (2022), 102375.

Gerke, H.H., and van Genuchten, M.T.: Macroscopic representation of structural geometry for simulating water and solute movement in dual-porosity media. *Advances in Water Resources*, *19*, (1996), 343–357.

Houseworth, J. E., Asahina, D., Birkholzer, J. T.: An analytical model for solute transport through a water-saturated single fracture and permeable rock matrix, *Water Resources Research*, 49, (2013), 6317– 6338.

Huang, J., Griffiths D.V., and Wong, S.W.: Characterizing Natural-Fracture Permeability from Mud-Loss Data, *SPE Journal*, March, (2011), 111-114.

Leij, F. J., Priesack, E., Schaap, and Marcel, G.: Solute transport modeled with Green's functions with application to persistent solute sources. *Journal of Contaminant Hydrology*, *41*(1-2), (2000), 155–173.

Maloszewski, P., and Zuber, A.: On the theory of tracer experiments in fissured rocks with a porous matrix. *Journal of Hydrology*, *79*(3-4), (1985), 333–358.

Rose, P.E., Benoit, W.R., and Kilbourn, P. M.: The application of the polyaromatic sulfonates as tracers in geothermal reservoirs. *Geothermics*, *30*(6), (2001), 617-640.

Sauty, J.-P.: An analysis of hydrodispersive transfer in aquifers, *Water Resources Research*, *16*(1), (1980), 145– 158.

Somogyvári, M., and Bayer, P.: Field validation of thermal tracer tomography for reconstruction of aquifer heterogeneity. *Water Resources Research*, 53(6), (2017), 5070-5084.

Şimsek, Ş.: Hydrogeological and isotopic survey of geothermal fields in the Buyuk Menderes graben, Turkey, *Geothermics*, *32*, (2003), 669-678.

Şimşek, Ş., Yıldırım, N., and Gülgör, A.: Developmental and environmental effects of the Kızıldere geothermal power project, Turkey, *Geothermics*, 34 (2), (2005), 234-251.